Journal of Sound and Vibration (1997) **204**(5), 755–768

AN EXPERIMENTAL STUDY OF THE ANGULAR DEPENDENCE OF LAMB WAVE EXCITATION AMPLITUDES

J. J. Ditri

1401 *Disston Street*, *Philadelphia*, *Pennsylvania* 19111, *U.S.A.*

AND

K. Rajana

Rosemount Aerospace, *Inc.*, *Eagan*, *Minnesota* 55121, *U.S.A.*

(*Received* 2 *August* 1996, *and in final form* 3 *January* 1997)

The generation of Lamb waves in isotropic layers by phase matching of an obliquely incident, bounded beam is examined experimentally, and the results compared to theoretical predictions obtained from a simplified model of the process. It is demonstrated experimentally that the range of incident angles over which any given mode can be generated is dependent upon the size of the transducer used to excite the mode, its frequency content and the pressure distribution across its surface. Experimentally obtained excitation amplitude versus incident angle curves are given for various Lamb wave modes and transducers of different sizes and vibrational characteristics. These experimental amplitudes are compared to theoretical curves based on a simplified model of the generation process.

1. INTRODUCTION

The use of an obliquely incident, bounded ultrasonic beam for the generation of Lamb waves in isotropic layers was analyzed both theoretically and experimentally by Viktorov *et al*. [1], in 1965. The main parts of the work were later reproduced in Viktorov's book on Rayleigh and Lamb waves [2]. Of several detailed observations made in these investigations, one was that for optimal generation of a mode of a given wavenumber, k, the angle of incidence should be "in the neighborhood" of the Snell's law angle, $\theta_i = \sin^{-1}(k/k_w)$, where k_w represents the wavenumber of the wave in the incident medium [2]. Such a choice of incident angle was being used by experimentalists utilizing Lamb waves for non-destructive evaluation purposes [3–5] even before Viktorov's analysis. The use of such an angle no doubt arose from the theory of (infinite) plane wave reflection/refraction at planar interfaces. In those cases, which are primarily of academic interest of for *approximating* real experimental conditions, Snell's law holds *exactly* as a result of satisfaction of boundary conditions along the entire (infinite) interface.

Another result of Viktorov's analysis, which forms the basis for the current study, was that for excitation by an incident beam of finite width there is actually a *continuous dependence* of the excitation amplitude of any mode on the angle of incidence. This can be understood if it is recalled that an incident *beam* is equivalent to a continuous spectrum of incident plane waves whose wave vectors are distributed about the central wave vector of the incident beam. The amplitude of each plane wave component ultimately determines the excitation strength of the guided wave modes.

0022–460X/97/300755 + 14 $25.00/0/sv970976

It should be noted that beam spreading was completely neglected in Viktorov's (and the present) analysis and hence the continuous dependence of the excitation amplitude of a given mode on the angle of incidence is *not* due to beam spreading. Beam spreading gives rise to additional physical phenomena, as discussed by Zeroug *et al*. [6].

In this paper, the phase matching method of generating guided waves is re-analyzed, with particular attention being focused on the relationship between the angularly dependent excitation amplitude of a given mode and the physical parameters of the transducer used to excite the mode. Most of the theoretical analysis relies on an extension of Viktorov's work to encompass arbitrary transducer pressure distributions and generally anisotropic layers [7]. Additional details of the present work can be found in references [8, 9]. This paper presents a more in-depth and systematic treatment of the posed problem.

2. ANALYSIS

Two common arrangements for implementing the phase matching method are shown in Figure 1. In the immersion approach, the layer is immersed in a fluid bath; whereas in the contact method, a (usually non-viscous) couplant is used to couple ultrasonic energy from an angled wedge into the layer. In either case, a finite sized transducer emits a beam of ultrasonic waves which subsequently impinges on, and generates waves in, the layer. The pressure profile across the face of the incident beam is denoted by $p(\alpha)$, with α denoting a co-ordinate parallel to the transducer face (i.e., perpendicular to the beam axis).

The incident beam will cause longitudinal and transverse waves to be excited in the layer, each with their own excitation amplitudes. For observation distances sufficiently far from the excitation region, the collection of generated and multiply mode converted waves in the layer can be most efficiently interpreted, both mathematically and conceptually, as a summation of the guided wave modes permissible in the layer with certain amplitudes [10].

An analysis of a two-dimensional model of the phase matching method (also known as the "wedge" method), applicable to arbitrary pressure distributions and generally anisotropic layers has recently been carried out [7]. In this analysis, the transducers were

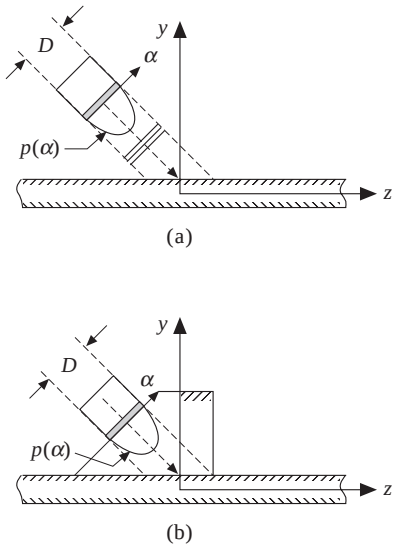

Figure 1. Schematic illustrations of (a) the immersion, and (b) the contact methods of generating Lamb waves using obliquely incident ultrasonic beams.

assumed to be infinite in one dimension, thus creating a state of plane strain deformation in the layer. Most of the analysis in reference [7] was focused on the time harmonic case, althought the effect of incident *pulses* was also briefly considered. The main assumption which was made in reference [7] was that the effect of the incident beam on the layer was equivalent to a prescribed traction distribution over the area of the layer insonified by the incident beam. The prescribed traction distribution was taken to be equal to that which would be produced by the incident beam alone. While this assumption considerably simplifies the boundary value problem, it restricts the applicability of the results to cases in which the medium containing the incident beam has a small acoustic impedance relative to that of the layer. This is essentially the same assumption made by Viktorov [1, 2].

Denoting by $A_v(z, \omega, \theta_i)$ the "z" dependent amplitude with which any propagating Lamb wave mode "v" of the layer is excited by the incident beam of frequency ω and incident angle θ_i, it was shown that,

$$A_v(z, \omega, \theta_i) = \frac{\tilde{v}_{vy}(b/2)}{4P_{vv}} \frac{e^{-ik_v z}}{\cos(\theta_i)} \int_{-\infty}^{\infty} p(\alpha)\, e^{i\chi\alpha}\, d\alpha, \tag{1}$$

where

$$\chi \triangleq \frac{k_v - k_w \sin\theta_i}{\cos\theta_i}. \tag{2}$$

In equation (1), $\tilde{v}_{vy}(b/2)$ denotes the complex conjugate of the "y" component of the particle velocity of mode "v" at the top surface of the layer (where $y = b/2$) and P_{vv} denotes the time average power flux carried along the layer by the mode v per unit waveguide width. The function $p(\alpha)$ represents the variation of the pressure over the width of the incident beam.

For symmetric Lamb wave modes, the out of plane particle velocity at the top surface of the layer can be expressed as [11]

$$v_{vy}(\omega, b/2) = -k_{tl} \sin(k_{tl}b/2) \cos(k_{ts}b/2) + \frac{k_{ts}^2 - k_v^2}{2k_{ts}} \cos(k_{tl}b/2) \sin(k_{ts}b/2), \tag{3}$$

whereas for anti-symmetric modes, the out of plane particle velocity at the top surface can be expressed as,

$$v_{vy}(\omega, b/2) = k_{tl} \cos(k_{tl}b/2) \sin(k_{ts}b/2) + \frac{k_v^2 - k_{ts}^2}{2k_{ts}} \sin(k_{tl}b/2) \cos(k_{ts}b/2). \tag{4}$$

The time average power flux (per unit width) of mode v is given by [11, p. 159],

$$P_{vv} = -\tfrac{1}{2}\, \mathrm{Re} \int_{y=-b/2}^{b/2} (\tilde{\mathbf{v}}_v \cdot \mathbf{T}_v) \cdot \hat{\mathbf{e}}_z\, dy. \tag{5}$$

In these expressions, the "transverse wavenumbers", k_{tl} and k_{ts} are defined as $k_{ts}^2 = (\omega/v_s)^2 - k_v^2$ and $k_{tl}^2 = (\omega/v_l)^2 - k_v^2$, with v_s and v_l representing the shear and longitudinal wave velocities, respectively. In addition, $\mathbf{T}_v$ denotes the stress tensor of mode v, $\hat{\mathbf{e}}_z$ denotes a unit vector in the z (propagation) direction, and Re denotes the real part. Both v_{vy} and P_{vv} are functions of frequency, ω or, alternatively, of the point on the dispersion curve at which mode v is generated.

The dependence of the modal amplitude, $A_v(z, \omega, \theta_i)$, on the wedge angle is partially explicit in equation (1) in the $\cos(\theta_i)$ term, and partially implicit through the χ terms in

the integral. The integral can be recognized as the Fourier transform of the applied traction distribution, $p(\alpha)$, with (real) transform parameter χ.

To make the dependence of the excitation amplitudes on incident angle completely explicit, a specific form must be assumed for the transducer pressure distribution, $p(\alpha)$. In the experimental work reported in later sections, the actual pressure distributions of several transducers were measured and used in equation (1), which was then numerically integrated to obtain $A_v(z, \omega, \theta_i)$.

To proceed further analytically, however, with the goal of understanding the physics of the excitation process through a simple approximation, it is assumed that the transducer produces a parabolic pressure distribution of the form,

$$p(\alpha) = \begin{cases} p_0 \left(1 - \dfrac{\alpha^2}{(D/2)^2}\right), & \text{if } |\alpha| \leqslant D/2, \\ 0, & \text{if } |\alpha| > D/2, \end{cases} \tag{6}$$

where p_0 represents the maximum pressure which occurs at the center of the transducer face, $\alpha = 0$, and the transducer has a width D. Substituting this pressure distribution into equation (1) and evaluating the integral yields for the amplitude of generic mode "v",

$$A_v(z, \omega, \theta_i) = \frac{2p_0 \tilde{v}_{vy}(b/2)\, \mathrm{e}^{-ik_v z}}{P_{vv} D \cos(\theta_i) \chi^2} \left[\frac{2 \sin(\chi D/2)}{D\chi} - \cos(\chi D/2)\right]. \tag{7}$$

Equation (7) can be used to predict the excitation amplitude of any propagating Lamb wave mode given the transducer and wedge parameters such as frequency (ω), transducer width (D) and incident angle (θ_i).

For a given frequency, there will be a finite number of real wavenumbers, k_v, $v \in \{1, 2, 3, \ldots\}$, corresponding to symmetric and antisymmetric Lamb wave modes, satisfying the dispersion equation of the layer. Using a particular wavenumber in equation (7), and calculating $v_{vy}(b/2)$ and P_{vv} for that mode, at the given frequency, reduces the right side to a function of θ_i alone, for given z and beam width, D. Of course, several propagating (and non-propagating) modes may be simultaneously excited by the incident beam and, therefore, the total field in the layer will correspond to a summation over all of the modes of the layer at the given frequency.

As an example of the use of equation (7) to predict the excitation amplitudes of Lamb waves for given transducer and wedge parameters, consider a 1·5 MHz transducer of a given size D, insonifying a 1·0 mm aluminum layer, with assumed longitudinal and shear wave speeds of 6·3 and 3·1 mm/μs, respectively. For the given frequency thickness product of 1·5 MHz mm, only the A_0 and S_0 modes propagate in the layer (see Figure 4). In Figure 2 is shown the predicted normalized excitation amplitudes of the A_0 and S_0 modes as functions of the "Snell's law phase velocity" and incident angle, for three different size transducers, viz., $D = 12{\cdot}7$ mm (1/2 inch), 38·1 mm (1·5 inch) and 254 mm (10·0 inch). The "Snell's law phase velocity" is defined as $V_{ph}^0 \triangleq v_w/\sin(\theta_i)$, where v_w represents the longitudinal wave speed in the wedge or immersion liquid (which was assumed to be 1·5 mm/μs, thus simulating water).

The curves have been simultaneously normalized so that the maximum value attained by either modal amplitude is unity. Note that the *incident angle* scale on the bottom decreases towards the right in a non-linear manner, since the Snell's law phase velocity scale, which is related to the sine of the incident angle, is linear.

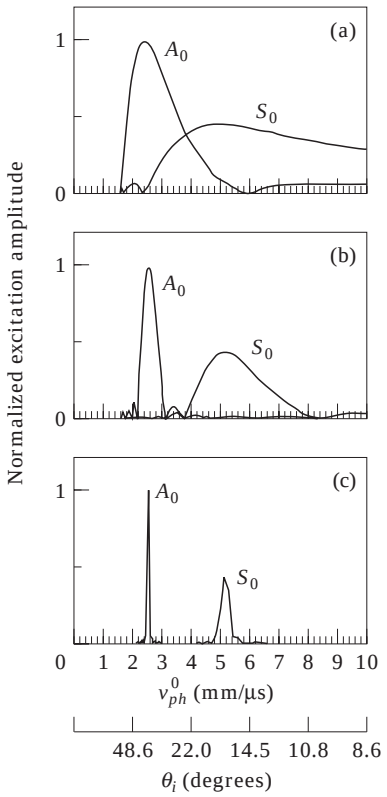

Figure 2. Theoretically predicted excitation amplitudes of the A_0 and S_0 modes, at $fd = 1{\cdot}5$ MHz mm, as a function of the Snell's law phase velocity, V_{ph}^0 (see equation (9)) and the incident angle, θ_i. (a) Beam width, $D = 12{\cdot}7$ mm; (b) $D = 38{\cdot}1$ mm; (c) $D = 254$ mm.

There are several features of the plots in Figure 2 which deserve mentioning. First of all, for a frequency thickness product of 1·5 MHz mm, the phase velocities of the S_0 and A_0 modes in an aluminum layer are 5·14 and 2·54 mm/μs, respectively. Using Snell's law, this gives maximum excitation angles of 17 and 36 degrees (using $v_w = 1{\cdot}5$ mm/μs for the incident velocity) respectively. As can be seen from Figure 2, the excitation spectra do indeed have maxima very close to these values.† This becomes particularly clear for the larger diameter transducers.

A second feature to note is that the maximum excitation amplitude of the A_0 mode is, at this frequency thickness product, larger than the maximum excitation amplitude of the S_0 mode. This has to do with the fact that the A_0 mode, at the given fd, has a predominantly out of plane particle displacement and is, therefore, efficiently generated by the normal traction which the incident wave applies to the layer. The S_0 mode, on the other hand, with its predominantly in plane particle motion (at the given fd), does not couple as efficiently to the normally applied pressure field. Thirdly, note that even for the same size transducer, the *width* of the excitation spectrum of the A_0 mode is narrower than that of the S_0 mode. This is essentially due to the fact that at the given frequency thickness

† It can be shown by differentiating equation (1) with respect to θ_i and taking the limit as $\theta_i \rightarrow \sin^{-1}(k_v/k_w)$, that $A_v(z, \omega, \theta_i)$ is *not* a maximum at the Snell's law angle. The actual maximizing angle is, however, generally very close to this angle.

product, the wavelength of the A_0 mode ($\lambda_{A_0} = 1{\cdot}7$ mm) is roughly one half that of the S_0 mode ($\lambda_{S_0} = 3{\cdot}4$ mm).

One can also note that the width of each excitation spectrum decreases as the size of the transducer, D, increases. It can be shown [7] that the width of the excitation spectrum (considered a function of the Snell's law phase velocity) normalized by the Snell's law phase velocity itself can be written in the form

$$\frac{\Delta V}{V_{ph}^0} = \frac{(K/\pi)(\lambda^0/\bar{D})}{1 - (K/2\pi)^2(\lambda^0/\bar{D})^2}, \tag{8}$$

where ΔV represents the width of the excitation spectrum at its -9 dB point (i.e., where the amplitude drops by 1/e from its maximum), and K is a constant depending upon the pressure profile of the transducer. For a parabolic source, $K \approx 5{\cdot}852$, whereas for a piston source, $K \approx 4{\cdot}398$. Also, the other quantities appearing in equation (8) are,

$$\bar{D} \triangleq D/\cos(\theta_i), \qquad V_{ph}^0 \triangleq v_w/\sin(\theta_i), \qquad \lambda^0 \triangleq V_{ph}^0/f, \tag{9}$$

with $f = \omega/2\pi$ representing the frequency of the transducer. Note that the width of the excitation spectrum (as a function of Snell's law phase velocity) is only a function of the dimensionless parameter $\lambda^0/\bar{D}$. Recognizing $\bar{D}$ as the length of the region over which the incident beam contacts the layer, it can be concluded that the width of the "phase velocity spectrum" is only dependent upon the ratio of the loading length to the wavelength of the mode being generated evaluated at the Snell's law phase velocity, V_{ph}^0.

The width of the phase velocity spectrum is directly related to the potential phase velocity measurement error which could occur when using goniometric techniques such as the leaky Lamb wave technique to measure phase velocities of guided waves. It is customary when using such techniques to infer the phase velocity of generated modes from the incident angle of the insonifying transducer using Snell's law. As shown by Figure 2, however, modes may be excited with appreciable amplitudes even if the incident angle does not satisfy Snell's law. It is therefore important to consider finite source effects in addition to angular positioning errors when estimating potential phase velocity errors using the phase matching technique.

Figure 3 is a plot of $\Delta V/V_{ph}^0$ as a function of $\lambda^0/\bar{D}$ for a source with parabolic pressure variation. As can be seen, in order to keep the width of the phase velocity spectrum to within 10% of the predicted Snell's law phase velocity, the insonification region must be at least 20 times larger than the wavelength of the mode being generated. This number will, in actual experimental arrangements, be reduced somewhat due to the spreading of

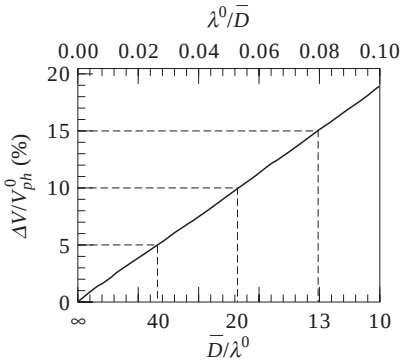

Figure 3. The relative width of the phase velocity spectrum versus the ratio of loading length ($\bar{D}$) to the Snell's law wavelength, λ_0 (see equation (9)).

the incident. Beam spreading will, among other things, increase the size of the insonification region.

There are, therefore, at least two sources of error in the goniometric measurement of phase velocity; i.e., errors in the actual incident angle, and errors due to finite source effects. In general, on the basis of our numerical calculations, the errors due to finite source effects are almost always at least an order of magnitude larger than those due to errors in incident angle. This is due mainly to the high accuracy of angular positioning systems currently available.

For a given layer thickness, the wavelength of any given mode varies, in general, from point to point on the mode's dispersion curve. A given size transducer will therefore be more or less selective to a given mode depending on where on its dispersion curve it is generated. There are, therefore, regions of the dispersion curves where, due to small wavelengths, the finite size of the transducer is not of great importance. On the other hand, some regions of the dispersion curves represent very large wavelengths and therefore the selectivity of even large (one inch, say) transducers to a particular phase velocity is very low. As an example, in Figure 4, is shown the -9 dB width of the phase velocity spectra at various points on the dispersion curves of different modes. The layer properties were that of aluminum ($V_L = 6{\cdot}3$ mm/μs, $V_T = 3{\cdot}1$ mm/μs, $\varrho = 2{\cdot}76$ g/cm^3) and its thickness was 1·0 mm. The size of the transducer used was $D = 12{\cdot}7$ mm, and the longitudinal wave speed of the wedge was 1·5 mm/μs. The vertical bars represent the range of incident angles over which the amplitude of the particular mode would be greater than -9 dB of the maximum, which occurs when the incident angle is chosen according to Snell's law.

As can be seen from Figure 4, for a given fixed frequency, the width of the excitation spectra *decreases* as the incident angle increases (or phase velocity decreases). This is due to the fact that as the incident angle increases, the insonification region increases and simultaneously, the phase velocity decreases, both giving rise to an *increase* in the ratio of $\bar{D}$ to λ^0. The width of the excitation spectra also decreases as the frequency increases for a given incident angle (or phase velocity). This is due to the decreasing wavelength with increasing frequency.

In the following sections, the details and results of an experimental program designed to assess the validity of the previous conclusions will be discussed.

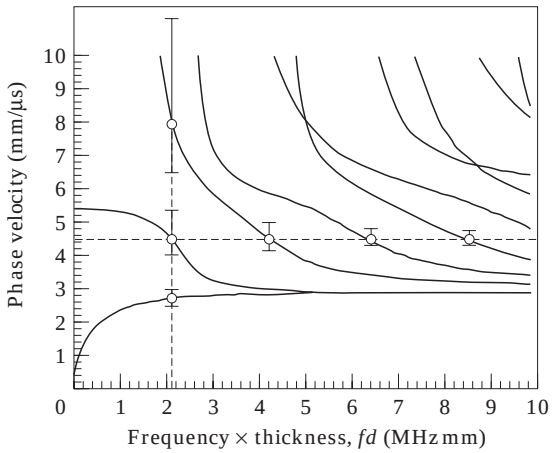

Figure 4. The dispersion curves of an aluminum layer. The vertical bars represent the theoretical -9 dB widths of the phase velocity spectra for various modes, using the *same size transducer* of $D = 12{\cdot}7$ mm.

3. EXPERIMENTAL APPARATUS

In this section, we report on experiments aimed at assessing the validity of the theory presented in the previous sections. A direct measurement of the pressure variation across the transducer face, $p(\alpha)$, was performed for several transducers of varying frequencies and nominal sizes. Using the measured profiles, equation (1) was numerically integrated to obtain theoretical predictions for the variation of the excitation amplitude of a given mode as a function of the incident angle of the transducer. The actual variation of excitation amplitude of several modes was directly measured using a novel experimental arrangement, and the results were compared to the theoretical predictions. Although beam spreading was neglected in the theoretical analysis, it was partially accounted for in the experiments because the "actual" transducer sizes (D_a) were taken as the -14 dB points in the experimentally obtained $p(\alpha)$ curves. Due to beam spreading, this width exceeded the physical (nominal) size of the transducer.

The modes/points chosen for study are listed in Table 1. The choice of these points is based upon consideration of the excitability of the modes and in an attempt to maximize the group velocity. The chosen points cover a moderate range of frequencies and wavelengths. To isolate an individual mode for the purposes of theoretically generating the excitation amplitude versus incident angle curve, that mode's wavenumber k_v, particle velocity field at the surface of the layer $\tilde{v}_{vy}(b/2)$ and the power flux P_{vv} were calculated for a frequency equal to the center frequency of the transducer used. This information was then used, along with the experimentally measured pressure profile of the transducer, in equation (1).

Standard, commercially available transducers of two different nominal frequencies (1·0 and 2·25 MHz) were used in this study. Three 1·0 MHz transducers and two 2·25 MHz transducers of different diameters were used. All transducers had circular piezoelectric elements with nominal diameters ranging from 6·35 to 19·05 mm. The transducers were driven by approximately ten cycles of a (rectangular) gated sinusoidal tone burst with a center frequency of 0·9 MHz for the 1·0 MHz nominal transducers and 2·25 MHz for the nominal 2·25 MHz transducers. The chosen number of cycles was sufficient to ensure a frequency bandwidth of less than 15% at the -6 dB level. The use of a rectangular gate caused the presence of side lobes in the frequency spectrum which were, in all cases, at around a -15 dB level compared to the principal maximum. High precision computer controlled linear translation and rotation stages were used to perform the experiments. The data acquisition system included a 100 MHz Sonix STR8100 digitizer and an NCR 386 personal computer.

TABLE 1

Modes used in the experimental study and some of their acoustical properties

Mode	fd (MHz mm)	V_{phase} (mm/μs)	Wavelength (mm)
S_0	0·914	5·38	5·8
S_0	1·013	5·30	2·4
S_1	4·572	5·78	2·6
S_2	7·143	6·47	2·9

TABLE 2

Nominal and "actual" diameters of the five transducers tested

Frequency (MHz)	Nominal diameter (mm)	Actual diameter, D_a(mm)
0·90	19·05	27·69
0·90	12·70	21·00
0·90	9·52	18·65
2·25	12·70	15·68
2·25	6·35	9·72

4. TRANSDUCER CHARACTERIZATION

The five transducers used in this study were first characterized by experimentally measuring the pressure profiles across their diameter. In an immersion tank, the transducer was used as a sender and a roughly 1 mm diameter pin-ducer, located at twice the near field of the sender, was used as a receiver. After locating the maximum in the pressure profile (at the center of the transducer) the transducer was traversed over a 20 mm distance with a 0·2 mm increment on either side of the maximum, giving a total of 400 points and 40 mm scan length. The data was smoothed by replacing each measured point with the average of it with its nearest two neighbors; a process which was done twice. The profiles were then normalized to unity maximum by dividing by the maximum value. The data points on the left and right of the maximum with amplitudes below 0·2 (i.e., -14 dB) were forced to decay exponentially with distance from the center. This was done to remove the electrical noise which was present at this low amplitude level. The width of the profile at the 0·2 (-14 dB) level was called the "actual" size of the transducer, D_a. The actual diameters are listed, along with the nominal (physical) size in Table 2 for the five transducers tested. Shown in Figure 5 are two typical measured profiles processed in this manner.

A cubic spline interpolant was numerically obtained for each measured transducer pressure profile. This provided a numerical approximation to the experimentally obtained pressure distribution profiles, and served as $p(\alpha)$ in the integrand of equation (1). Utilizing

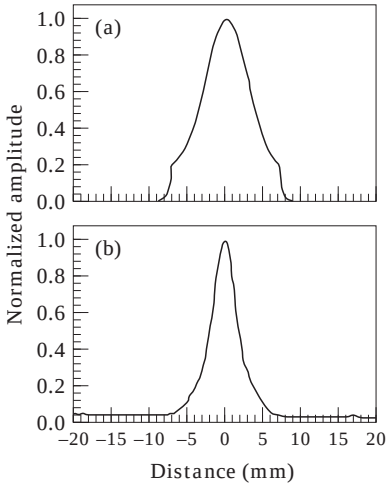

Figure 5. Two typical processed transducer pressure profiles: (a) 1·0 MHz transducer; (b) 2·25 MHz transducer.

the measured profiles, equation (1) was numerically integrated to obtain the predicted amplitude versus incident angle curves of specific Lamb wave modes.

5. DIRECT MEASUREMENT OF EXCITATION AMPLITUDES

In order to experimentally measure the excitation amplitude of a given mode for a given transducer, an immersion setup was employed. A plate of a given thickness (b) was mounted onto a computer controlled rotatable turntable which was immersed in a water tank. The transducer was also immersed and aligned relative to the plate so that the center of the emitted beam struck as nearly as possible the axis of rotation of the plate (Figure 6). The incident beam excited Lamb waves in the plate which propagated along the plate until reaching the end, where they were reflected and returned to the sender. The amplitude of the returning Lamb wave was detected by the transducer due to leakage into the surrounding water. The distance from the axis of rotation to the end of the plate was two inches (50·8 mm) in all cases. The distance from the transducer to the axis of rotation was twice the near field of the sender ($2N$), calculated based on the driving frequency and *nominal* diameter of the transducer.

The maximum amplitude in a gated portion of the received signal was recorded as the plate was rotated over a range of angles which depended upon the mode chosen. The angular increment in each case was 0·2 degrees. Care was required in gating the received signal to isolate a given mode since in many cases modes with nearly coincident phase velocities were excited. Time gates to isolate given modes were chosen according to theoretically calculated group velocities and known propagation lengths. This was not a problem in most cases, since differing group velocities caused separation of the modes, but it proved to be a problem when the group velocities of the generated modes was also similar.

In order to excite different modes, as well as the same mode with different wavelengths, while using only two different frequencies, aluminum plates of four different thicknesses were used. For the 0·9 MHz transducers, a 1·016 mm thick plate was used to isolate the S_0 mode at a frequency thickness product (fd) of 0·9144 MHz mm. The 2·25 MHz transducers were used on plates of 0·432, 2·032 and 3·175 mm to generate modes S_0, S_1 and S_2 at fd's of 1·01, 4·57 and 7·14 MHz mm, respectively. The experimentally obtained excitation amplitude versus incident angle curves were normalized to unity maximum in order to compare them to the theoretically generated curves.

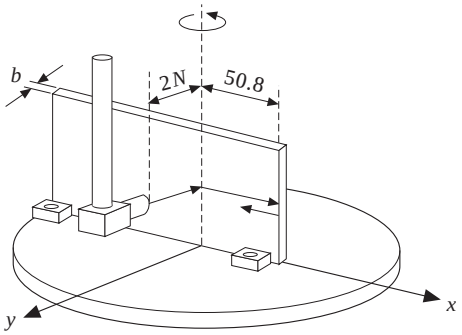

Figure 6. The experimental arrangement for monitoring the Lamb wave excitation amplitudes as functions of incident angle. The incident beam strikes an immersed plate along its axis of rotation, and the generated Lamb waves, after reflecting from the end of the plate, return to the sender.

6. RESULTS AND DISCUSSION

Results for the excitation of the S_0 mode in a 1·016 mm aluminum plate using three different size transducers, all driven at 0·9 MHz, are presented in Figure 7. The open circles connected by dashed lines represent the experimentally obtained profiles and the solid lines represent theoretical curves. For all of the results to be presented, data was collected in 0·25 degree increments, but for clarity of presentation, not all of the data points are shown by open circles. The lines connecting the open circles are *actual data points*, not interpolations between data points.

Note that the normalized excitation amplitudes are plotted versus the incident angle using a *linear* scale for the angle, not the non-linear scale used in previous figures. Because of uncertainty in absolute measurement of incident angle, the theoretical curves were shifted when necessary (in no case by more than 1 degree) to make the principal maxima of the theoretical and experimentally obtained curves coincide.

Several observations can be made concerning these results. First, there is good overall agreement between theory and experiment for the 27·69 (a) and 21·00 mm (b) transducers, whereas the experimental curve for the 18·65 mm transducer (c) is considerably wider than the theoretically predicted curve. Each set of experiments was performed twice to assess repeatability, which was excellent in all cases. The sets of amplitude profiles which were obtained on subsequent runs were, apart from small shifts in the angle, indistingushable from one another.

Notice that as the (actual) size of the transducer decreases, the widths of both the theoretical and experimental profiles increase. It may be noted that in this set of

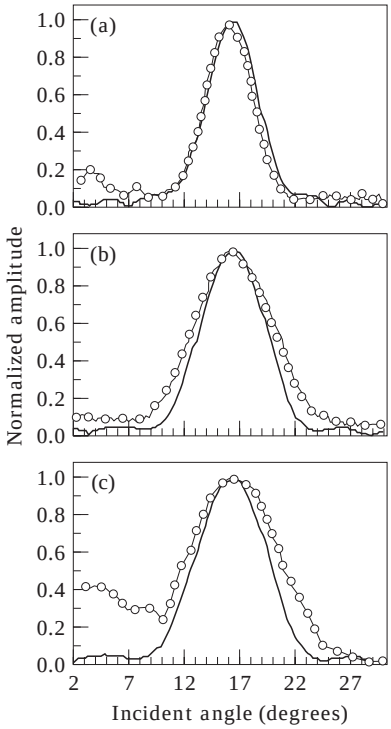

Figure 7. Theoretical (solid line) and experimental (light line, open circles) excitation amplitude versus incident angle curves for the S_0 Lamb wave mode, at a frequency–thickness product of $fd = 0{\cdot}9144$ MHz mm. All theoretical and experimental curves have been normalized to unity for comparison. (a) Actual transducer width, $D_a = 27{\cdot}69$ mm; (b) $D_a = 21{\cdot}0$ mm; (c) $D_a = 18{\cdot}65$ mm.

experiments, the only variable is source size; the other critical parameters such as Snell's law angle (based on the S_0 mode phase velocity at the given fd product), excitation frequency (hence the wavelength in the plate, λ^0) and the wavelength in the coupling medium being held constant.

The $-1{\cdot}80\%$ and $12{\cdot}26\%$ difference between the -6 dB widths of the theoretical and experimental profiles for the sources of 27·69 and 21·00 mm, respectively, are considered acceptable, especially considering differences between theoretical assumptions and the actual experimental setup. The difference associated with the source of 18·65 mm is 53·0% and this is considered too large to attribute to experimental error. It is believed that beam spreading effects, which have been neglected in the theory but are of course present in the experiment, play a major role in the deviation. Beam spreading effects become more important when either the nominal size of the transducer or its driving frequency decrease. Based on the nominal diameters of the transducers used in cases (a), (b) and (c), along with the driving frequency of 0·9 MHz, and a speed in water of 1·5 mm/μs, the half-angles of beam divergence calculated using the standard formula $\sin(\alpha) = 0{\cdot}6v_{water}/fD$ are $\alpha = 3{\cdot}0$, 4·5, and 6·0 degrees, respectively.

In a second set of experiments, the S_0 mode was generated at an fd product of 1·0125 MHz mm using a 2·25 MHz transducer and an aluminum plate of 0·432 mm thickness. This is nearly the same point as generated in the previous experiments (with $fd = 0{\cdot}9144$) but the frequency was more than doubled and the plate thickness was correspondingly less than half, so that fd was kept roughly the same. A transducer with an actual (measured) diameter of $D_a = 15{\cdot}68$ mm was used. The measured and theoretically predicted amplitude profiles are shown in Figure 8(a) along with a repetition of Figure 7(b), which, as mentioned, corresponds to roughly the same point on the S_0 mode dispersion curve, but which had roughly half the frequency (and double the plate thickness).

This comparison shows that it is not only the *size* of the transducer which determines the width of the angular spectrum but its *frequency* as well: the higher the frequency, the

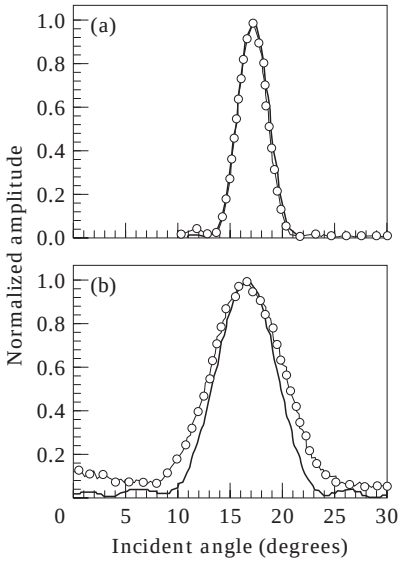

Figure 8. Theoretical (solid line) and experimental (light line, open circles) excitation amplitude versus incident angle curves for the S_0 Lamb wave mode generated at roughly the same frequency thickness product using different frequencies and layer thicknesses. (a) $f = 2{\cdot}25$ MHz, layer thickness, $d = 0{\cdot}432$ mm, therefore, $fd = 1{\cdot}0125$ MHz mm; (b) $f = 0{\cdot}9$ MHz, layer thickness, $d = 1{\cdot}016$ mm, therefore, $fd = 0{\cdot}9144$ MHz mm.

narrower the width of the angular amplitude excitation profile. Notice that this effect is captured remarkably well in the theoretical prediction with a difference between the -6 dB widths from theory and experiment of less than 5%. The half angle of beam divergence for the 2·25 MHz transducer with a nominal diameter of 15·68 mm is $\alpha = 1{\cdot}8$ degrees.

Note also that although the actual diameters of the transducers used to generate Figures 8(a) and 8(b) are around 25% different, this difference in size would cause the opposite effect as that which has occurred (i.e., it would tend to make the two widths closer), showing that the dominant cause of the difference in width is due to the difference in frequency.

As a final set of experiments, 2·25 MHz transducers with actual diameters $D_a = 15{\cdot}68$ and 9·72 mm were used to generate modes S_1 and S_2 at frequency thickness products of 4·572 and 7·143 MHz mm, respectively. The experimental and theoretical amplitude profiles are shown in Figure 9. Note that there are two peaks present in the experimental curves of Figure 9. This is due to the simultaneous excitation of S_1 and S_2. The theory curve has been generated assuming excitation of only S_1 and therefore has only one peak. Similar observations can be made concerning these profiles as has been made concerning the others. The width of the amplitude profile of any given mode increases as the actual size of the transducer decreases. The agreement between theory and experiment generally degrades as either the nominal size or the driving frequency of the transducer decreases. Both of these effects cause larger beam spreading which has been completely neglected in the theory.

It should be mentioned that satisfactory agreement has been obtained between the theory developed in reference [7] and the current experiments even though the theory was developed for *traction free* layers, whereas the layers used in the experiments were immersed in fluid. Several reasons can be given for the agreement. First of all, the experiments were performed using water-loaded aluminum plates. Because of the small acoustic impedance of the fluid relative to that of the plates, the characteristics of the modes will not, in general, be greatly affected. Secondly, and perhaps more importantly, in all of the comparisons of theory to experiment, only *normalized* excitation amplitudes

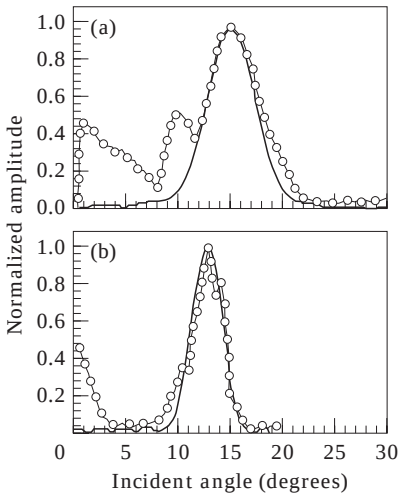

Figure 9. Theoretical (solid line) and experimental (light line, open circles) excitation amplitude versus incident angle curves for the S_1 and S_2 Lamb wave modes. (a) S_1 at $fd = 4{\cdot}572$ MHz mm ($f = 2{\cdot}25$ MHz, $d = 2{\cdot}032$ mm) with a transducer of actual diameter, $D_a = 9{\cdot}72$ mm; (b) S_2 at $fd = 7{\cdot}143$ MHz mm ($f = 2{\cdot}25$ MHz, $d = 3{\cdot}175$ mm) with a transducer of actual diameter, $D_a = 15{\cdot}68$ mm.

are compared. Both the theoretical and experimental amplitudes have been (independently) normalized to unity maximum. Therefore, although the *absolute* excitability of any given mode (i.e., the degree of coupling of the incident beam to the given mode) would change depending on whether the mode was generated in an immersed or free layer, the normalized curves would remain relatively unchanged.

7. CONCLUSIONS

Based on the comparisons of theory to experiment for all of the cases presented, it is concluded that the theory developed in reference [7] gives satisfactory results for predicting the width of the excitation spectrum of a given Lamb wave mode using a particular transducer. The discrepancy between theoretically predicted and experimentally obtained results increases as the beam spread of the source transducer increases. Beam spreading causes both a widening of the beam waist *and* a system of non-parallel rays in the incident beam. While the widening of the beam waist was accounted for by using the actual beam profiles in the numerical integrations, the non-parallel rays in the beam bundle were completely unaccounted for in the theory. Also not accounted for in the theory is the circular nature of the transducers used; in the theory, strip sources (two-dimensional) were assumed.

REFERENCES

1. I. A. Viktorov, O. M. Zubova and T. M. Kaekina 1965 *Soviet Physics—Acoustics* **10**(4), 354–359. Investigation of Lamb wave excitation by the wedge method.
2. I. A. Viktorov 1967 *Rayleigh and Lamb Waves*: *Physical Theory and Applications*. New York: Plenum Press.
3. D. C. Worlton 1957 *Nondestructive Testing* **15**(4), 218–222. Ultrasonic testing with Lamb waves.
4. D. C. Rasmussen 1958 *Nondestructive Testing* **16**(3), 228–236. Ultrasonic inspection of turbine and compressor blades for cracks and other flaws.
5. D. C. Worlton 1961 *Journal of Applied Physics* **32**(6), 967–971. Experimental confirmation of Lamb waves at megacycle frequencies.
6. S. Zeroug and L. B. Felsen 1994 *Journal of the Acoustical Society of America* **95**(6), 3075–3089. Nonspecular reflection of two- and three-dimensional acoustic beams from fluid-immersed plane-layered elastic structures.
7. J. J. Ditri and J. L. Rose 1994 *Transactions of the American Society of Mechanical Engineers*, *Journal of Applied Mechanics* **61**(2), 330–338. Excitation of guided waves in generally anisotropic layers using finite sources.
8. J. J. Ditri and K. Rajana 1995 *Review of progress in Quantitative Nondestructive Evaluation* Volume 14A (D. O. Thompson and D. E. Chimenti, editors), 163–170. New York: Plenum Press. Analysis of the wedge method of generating guided waves.
9. K. Rajana, J. J. Ditri, D. Hongerholt and J. L. Rose 1995 *Review of Progress in Quantitative Nondestructive Evaluation*, Volume 14A (D. O. Thompson and D. E. Chimenti, editors), 171–178. New York: Plenum Press. Analysis of the generation of guided waves using finite sources: an experimental approach.
10. I. T. Lu, L. B. Felsen and J. M. Klosner 1990 *Transactions of the American Society of Mechanical Engineers*, *Journal of Engineering Material Technology* **112**, 236. Beam to mode conversion in an aluminum plate for ultrasonic NDE applications.
11. B. A. Auld 1990 *Acoustic Fields and Waves in Solids*, Volume II, 83–84. Malabar, Florida: Kreiger; second edition.